Calcium Phosphate Decontamination of Stainless Steel Surfaces

Christine S. Grant, Gregory E. Webb, and Young W. Jeon
Dept. of Chemical Engineering, North Carolina State University, Raleigh, NC 27695

A primary constituent in high-temperature (120 – 140°C) milk fouling residues is calcium phosphate in the form of calcium phosphate dihydrate (brushite, $CaHPO_4 \cdot 2H_2O$) and hydroxyapatite [$Ca_5(PO_4)_3OH$]. The removal of these mineral-rich deposits from stainless steel occurs by dissolution and mechanical cleaning. This research uses a novel solid scintillation technique to noninvasively and continuously investigate the removal of P^{32}-labeled mixtures of calcium phosphate from inner surface of stainless steel tubes. The proposed mass-transfer model suggests that the film is initially removed by dissolution, when compared to the experimental results. An alternative first-order model presented includes the effects of the solvent flow rate and solvent pH on decontamination rates. This model agrees with the experimental cleaning data over the range of pH and flow rates studied.

Introduction

The fouling of heat-transfer surfaces in chemical processing equipment is a widespread problem in the chemical and food industry. Fouled heat-transfer surfaces increase costs for added heat-transfer surface area, energy losses, maintenance, and production losses caused by unit downtime. In the U. S., the costs associated with fouling in the food and chemical industry have been estimated to be \$1.8–2.9 billion/yr (Lund, 1981). A recent article by Sandu and Singh (1991) divides the costs into the following categories: (1) increased capital costs; (2) increased energy costs during operation; (3) maintenance costs (e.g., cleaning and treatment of resulting effluents); (4) production loses associated with plant downtime for cleaning; and (5) energy losses. They predicted that the cost associated with the cleaning of fouled heat exchangers in the fluid milk industry for 1990–91 was \$73 million/yr. This figure includes the energy required for the heating and circulation of the cleaning agents, labor, and cleaning agent costs. These economic and performance losses are the driving force for research on improved methods of cleaning fouled surfaces, prevention and reduction of fouling, and methods of measuring cleaning rates of fouled surfaces.

Cleaning contaminated surfaces in the food industry is exceptionally challenging because the heterogeneous nature of the residues that accumulate on solid surfaces makes it difficult for a single solvent or surfactant system to clean all surfaces completely. Most cleaning and sanitation procedures in the food industry consist of a series of cleaning steps (Plett, 1985), which may include prerinse, cleaning, interrinse, sanitizing, and postrinse. The prerinse step is used to remove large, loosely bound particles. The cleaning step removes residual soil by dissolution using a suitable solvent or detergent. The interrinse step removes residual detergent remaining from the cleaning step. Heat and/or disinfectants are used in the sanitizing step to destroy microorganisms. The postrinse removes any remaining cleaning agents. When only water is used in the postrinse, the operation is called rinsing and the cleaning effect is provided by the mechanical action and the solvency of water; if detergent solutions or sanitizers are used, the final process is called cleaning or sanitizing, respectively.

Cleaning in place (CIP) techniques involve the pumping of cleaning agents through processing units without dismantling the process equipment (Wennerberg, 1981). CIP procedures minimize the requirements of time, labor, cleaning solvent and energy associated with the disassembling of processing equipment. Although CIP procedures maintain cleaning efficiency, it is often difficult to verify the degree of internal surface cleanliness and the rate at which the surface is cleaned. Since cleanliness and cleaning rates are not always known in CIP processes, chemical and food industries often use cleaning reagents and solvents inefficiently (Perka et al., 1993).

Previous research methods have either interrupted the cleaning process or disturbed fluid flow in an effort to determine the amount of residue on a solid surface. In a study of

Correspondence concerning this article should be addressed to Christine S. Grant.
Current address of Y. W. Jeon: Dept. of Environmental Engineering, Kyungpook, National University, Taegu, Korea.

cleaning in the food industry, Corrieu states that there is an urgent need to develop an apparatus that would allow continuous, noninvasive measurement of cleaning phenomena (Corrieu, 1981). We have developed such a technique wherein the radioactivity of fouling deposits on the internal surface of a cylindrical flow cell is monitored continuously using solid scintillation.

This research examines the effects of pH, surface finish, and flow rates on the cleaning rates of calcium phosphate deposits on stainless steel surfaces representative of those found in milkstone (that is, milk fouling deposits). Dissolution and shear models are developed to describe the removal of calcium phosphate from a cylindrical hard surface into a flowing solvent. This research will assist the food process industry in the development of better methods of estimating milk deposit removal, and consequently a better understanding of the mechanisms that govern the removal of contaminants from hard surfaces.

Literature Review: Models and Techniques

Milk residue formation and cleaning

The primary constituents of milk dry matter are lactose (37.6%), fat (30.4%), protein (26.4%), and minerals (5.6%) (Lyster, 1979). Milk compounds are either water-soluble (whey proteins, carbohydrates, and salts), or insoluble (fat globules and casein micelles). Milk protein is composed of approximately 80% casein and 20% whey protein. The mineral portion of milk is composed of approximately 60% calcium phosphate and smaller amounts of magnesium, sodium and potassium salts.

Milk fouling is the result of chemical interactions between milk components and metal surfaces. Figure 1 shows the various conditions at which milk is processed and the deposits created under these conditions. At operating temperatures of approximately 100°C, the dry milk deposit is composed of 50 to 60% protein, 30 to 35% minerals, and 15 to 20% fat (Lalande, 1988). At temperatures from 130 to 140°C (e.g., during sterilization), the deposit (referred to as milkstone) has a high density and is composed of up to 75% minerals.

The mechanism of milk deposition on metal surfaces has been represented by several fouling models. A two-stage model describes the deposition of β-lactoglobulin, the most thermally labile milk protein, as taking place in induction and fouling periods (Gotham et al., 1989). A three-stage or defects-growth model (Figure 1b) considers the fouling behavior of milk proteins and mineral salts to occur in three steps: development of a compact sublayer, granule formation, and deposit growth (Sandu, 1989).

In the two-stage model induction period, a thin deposit layer of salts and proteins is formed on the metal surface. In the fouling period, insoluble protein aggregates form through a rapid homogeneous reaction in the bulk fluid. In the latter process, β-lactoglobulin partially unfolds in molecular denaturation at about 70°C, exposing disulfide and sulphydryl groups that are normally concealed within the core of the protein. Disulfide bridging between different denatured molecules can then occur, resulting in the formation of large polymerized and insoluble protein aggregates. These aggregates adhere to the deposit layer formed in the induction period, causing the deposit to grow.

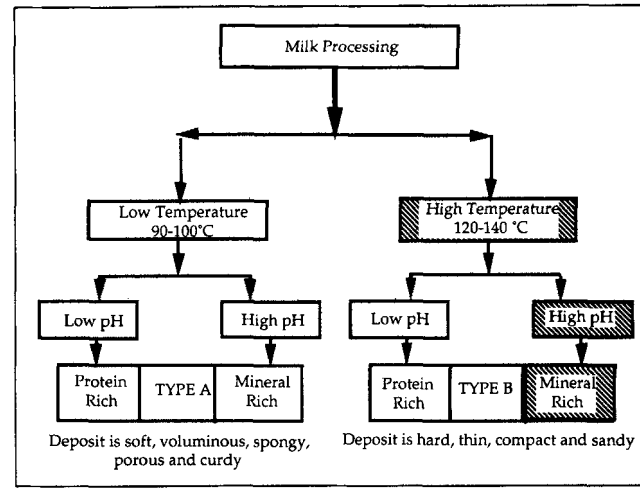

Figure 1a. Milk processing conditions.

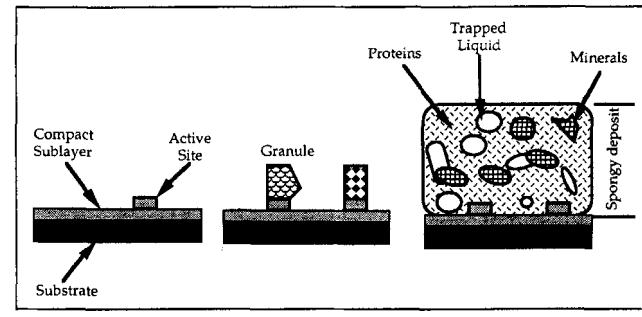

Figure 1b. Milk deposit growth.

Three stage deposit formation: compact sublayer, granule formation and spongy deposit (after Sandu, 1989).

In the three-stage model the compact sublayer formed at metal surfaces is composed of calcium phosphate and protein. Some active sites on the sublayer surface (called protuberances) provide anchors for the granules of large protein aggregates, leading to the growth of a porous, spongy deposit with low density and high moisture content. Some fat globules and microorganisms are also entrapped in this matrix.

Fouling can be described as a heterogeneous reaction that causes the aggregation of β-lactoglobulin, α-lactoglobulin, caseins, and fat globules to the surface. Calcium phosphate contributes to growth of the deposit by creating "carboxylate" bonds between protein aggregates and precipitated minerals. The most common mineral components appear to be calcium phosphate dihydrate (brushite) ($CaHPO_4 \cdot 2H_2O$) and octocalcium phosphates [$Ca_8H_2(PO_4)_6 \cdot 5H_2O$] with hydroxyapatite [$Ca_5(PO_4)_3OH$], the least soluble form, on the surface (Sandu and Lund, 1985). These minerals form readily on heat-transfer surfaces, because raw milk exhibits a high degree of supersaturation and due to the inverse-solubility of the calcium phosphates (Sandu and Lund, 1985).

Two cleaning processes are commonly used for milk residues: a two-stage process and a single-stage process (Timperley and Smeulders, 1987). In single-stage cleaning, the residues are removed by formulated detergents, which contain surface active agents and chelating agents. A single-stage process may also utilize a highly acidic or alkaline solvent. In the two-stage process, the proteins and fats are removed with

an alkaline solvent (e.g., NaOH) and the mineral deposits are removed by an acidic solution (e.g., HNO_3 or H_3PO_4). Many cleaning studies have focused on the removal of heterogeneous mixtures of fats and proteins as a function of alkali concentration (Grasshoff, 1989; de Goederon and Pritchard, 1989). The current research focuses on the removal of calcium phosphate, the mineral commonly found in high-temperature milk deposits, from stainless steel surfaces.

Cleaning models used in the food industry

The cleaning models used in the food industry range from purely empirical relationships to models based on mass-transfer principles. Jennings was one of the first to develop models to describe the removal of food products from solid surfaces (Jennings et al., 1957). He studied the effects of time, temperature, and solvent type (e.g., pH) on the removal of P^{32} radio-labeled dried milk from solid surfaces; the mass of the remaining film was determined by measuring the activity of the remaining sample. Measurements of the contaminant remaining were made by removing contaminated plates from the flow system. Jennings selected a second-order empirical model for the rate of removal of milk residues as a function of the concentration of hydroxyl ions ($C_{OH,B}$) like and the concentration of the contaminant to be removed (C_x):

$$\frac{dC_x}{dt} = -kC_xC_{OH,B} \tag{1}$$

where k is an empirical rate constant. Based on comparisons with experimental data, the model is only valid up to the removal of 60% of the initial contaminant. The lack of continuous measurements of the mass of contaminant made it difficult to make an accurate assessment of cleaning kinetics.

Bourne and Jennings (1962) expanded Jennings' original model to include two parallel first-order reactions to explain the marked decrease in the cleaning rate for stainless steel contaminated with tristearin. Bourne assumed this decrease was caused by differences in the binding energy between tristearin bound to tristearin and tristearin bound to the substrate. This conclusion was supported by experiments that varied the thickness of the contaminant film.

Harper suggested that the cleaning process proceeds in four stages (Harper, 1972):

Stage 1: Transport of the solvent to the surface of the contaminant to be removed.

Stage 2: Wetting and penetration of the deposit by solvent.

Stage 3: Transport of contaminant away from the solid-liquid interface.

Stage 4: Prevention of contaminant redeposition onto the clean, solid surface.

Although Harper's concept of the cleaning mechanism is extensive relative to Jennings work, it is difficult to model each stage theoretically. Schlussler attempted to simplify the mechanisms of Harper with the objective of developing a pragmatic model to describe cleaning behavior (Schlussler, 1970):

$$\frac{dN}{dt} = -\frac{D_{soil}A}{t_{boun}}(C_w - C_b) \tag{2}$$

where dN/dt is the number of moles dissolved per unit time, C_w is the concentration of contaminant in equilibrium with solvent, C_b is the concentration of soil in bulk solution, A is the surface area of soil, D_{soil} is the diffusivity of the contaminant in the solvent, and t_{boun} is the thickness of the equivalent boundary layer.

Schlussler's model assumed that the first and third stages in Harper's model were controlled by diffusional mechanisms across an equivalent hydrodynamic boundary layer created by the fluid stream. The model also assumed that: (1) the dissolved contaminant diffuses more slowly than the solvent itself; (2) the transport of contaminant away from the solid-liquid interface, stage three, was the rate-limiting step for the overall removal of contaminant. Schlussler calculated C_w by assuming it was equal to the concentration of the bulk solvent after the contaminant was completely removed. Although Schlussler's model is based on fundamental mass-transfer principles instead of an empirical relationship, he has been criticized for the approach used to calculate the concentration at the solid-liquid interface (Lenges, 1982; LeClercq-Perlat and Lalande, 1991).

One of the first attempts to develop a continuous, noninvasive technique for measuring the removal of contaminant films was made by Gallot-LaVallee et al. (1982), who used an optical detector to measure the turbidity of the solvent after it had passed the contaminated surface. They applied this technique to measure the decontamination of tubes fouled with milk deposits similar to those formed during pasteurization and proposed a new two-stage cleaning model:

$$\frac{dM}{dt} = b_5[1-\exp(b_6t)] \qquad \text{for } t < M_0/b_5, \tag{3}$$

$$\frac{dM}{dt} = b_5\{\exp[b_6(M_0/b_5)]-1\}\exp(-b_5t) \qquad \text{for } t > M_0/b_5, \tag{4}$$

where M_0 is the initial mass of the soil and b_5 and b_6 are rate constants. The first stage, a zero-order step, represents the formation of an intermediate component, analogous to an active site complex in a heterogeneous catalytic reaction. The second stage represents the removal of intermediate components through the equivalent concentration boundary layer. Gallot-LaVallee et al. suggest possible problems with the turbidity measurements taken downstream from the surface being cleaned. This lag in the turbidity measurements created a residence time distribution that further complicated analysis of their data.

Cleaning models developed for the chemical and nuclear industries

Models for the cleaning of contaminated solid surfaces have also been developed for the chemical and nuclear industries. Kern and Seaton's model explains in detail the fouling process and its effects on heat-transfer equipment in the nuclear industry (Kern and Seaton, 1959; Murray, 1987):

$$\frac{dM}{dt} = -k_1\tau t_{film}, \tag{5}$$

where k_1 is an arbitrary rate constant, τ is the shear stress at the interface, M is the mass of the deposit, and t_{film} is the thickness of the deposit. Kern and Seaton's model is based on the following assumptions: (1) the removal of contaminants is due to the shearing action of fluid passing the surface of contaminants; (2) the contaminant film is removed as chunks of material at random planes of weakness; (3) these planes of weakness are likely to occur at any depth. Incorporating the definition of shear stress, the rate of deposit removal becomes:

$$\frac{dM}{dt} \propto v^{1.75}. \tag{6}$$

Murray developed a model to describe the removal of oxide films (Murray, 1987a) based on an acidic solvent traveling through a solution mass-transfer film and dissolving the metal oxide covering the reactor surface. The model includes a moving interface between the solvent and the solute and assumes that dissolution occurs at the film surface and throughout the film. In this model, Murray makes the following assumptions: (1) a uniform solution and uniform oxide film; (2) small porosity changes throughout the oxide film; (3) quasi-steady state; (4) no bulk velocity contributions to mass transfer within the oxide film; (5) no corrosion of the base metal; (6) mass transfer in only one direction. Using these assumptions, Murray developed an expression for the thickness of the metal oxide film (z_w) during cleaning:

$$\frac{dz_w}{dt} = k_2 \exp(-kt) \tag{7}$$

where k and k_2 are rate constants based on physical parameters of the oxide film and the solvent. Initial oxide removal data shows higher-order kinetics that are not predicted by this model. Murray proposed that these deviations were a result of surface wetting, pore filling, and/or gas evolution.

The effects of solubility on mass transfer have been outlined in studies performed by Linton and Sherwood (1950) and Harriott and Hamilton (1965). In both of these studies, a solid material was compressed into hollow cylinders that were inserted into a flow system and a solvent in which the tubes were soluble flowed past the tubes. The solid tubes were compressed sufficiently enough that mechanical cleaning would not play a large role in the removal of material. These two studies have shown that even without the mechanical cleaning mechanism, solvent velocity plays a significant role in material removal. Murray's models accurately predict the removal of metal oxides from boiling water reactors by incorporating dissolution mechanisms (Murray, 1987a). These studies support the idea that cleaning can occur without large contributions from mechanical effects.

The importance of mechanical effects in cleaning has also been studied. Timperley studied the effects of velocity on cleaning rates of tenacious soils coated on the inside of stainless steel pipes with various diameters (Timperley, 1981). He concluded that it was shear stress that influenced the cleaning rates of his system. Studies performed by Jackson on the removal of tomato paste from heat exchanger plates found similar results (Jackson, 1984). Jackson found that significant cleaning required a minimum velocity; below the minimum velocity the fluid does not provide enough shear to remove a significant portion of the contaminant.

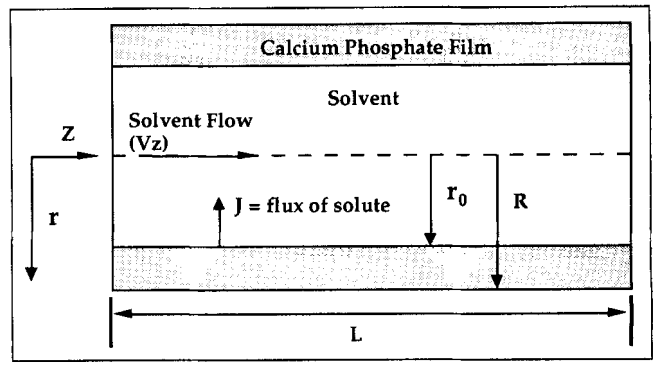

Figure 2. Control volume used as basis for dissolution model.

Many challenges still exist in the modeling of decontamination rates including the incorporation of surface morphology, effects of solvent additives (e.g., pH), the role of heterogeneous contaminants, and the geometry of the fouled surface into the models.

Dissolution Model of Calcium Phosphate Removal

The dissolution of calcium phosphate from the inside of a cylindrical surface can be described by a standard mass-transfer model (Figure 2). A balance performed on a differential volume element of solid within the pipe yields the local rate of change of the mass within the differential control volume:

$$\frac{\partial M'(z)}{\partial t} = -J(z)A\overline{M} \tag{8}$$

where A is the surface area of the control volume, and $\overline{M}$ is the average molecular weight of the material in the film. The molar flux J can be written as $J = -k_m(C_b - C_w)$ where C_b is the bulk concentration of calcium phosphate, C_w is the concentration of calcium phosphate at the solid-liquid interface, and k_m is the mass-transfer coefficient. Equation 8 becomes:

$$\frac{\partial}{\partial t}[\rho_o \Delta z \pi (R^2 - R_i^2)] = -J(z)\overline{M}2\pi R_i \Delta z \tag{9}$$

where ρ_o is the density of the calcium phosphate film, R is the radius of the cylinder, and R_i is the radius of the film at a given axial position and time. Rearrangement of Eq. 9 results in:

$$\frac{\partial R_i}{\partial t} = \frac{-k_m(C_b - C_w)\overline{M}}{\rho_o}. \tag{10}$$

The above expression for the radial position of the solid-fluid interface can be written in terms of dimensionless variables:

$$\frac{\partial \phi}{\partial \eta} = \frac{-k_m \overline{M} L}{\rho_o < v_z > r_o}\theta(Z, \eta) \tag{11}$$

where

$$\eta = \frac{t < v_z >}{L}, \quad \theta = (C_b - C_w), \quad \phi = \frac{R_i}{r_o}, \quad Z = \frac{z}{L}. \quad (12)$$

Here L is the length of the tube cell and r_o is the initial radius of the solid-liquid interface.

A balance on the solute in the liquid phase results in the following differential equation for the concentration θ

$$\frac{\partial \theta}{\partial \eta} + \frac{\partial \theta}{\partial Z} = -\frac{2k_m}{r_0}\frac{L}{< v_z >}\theta. \quad (13)$$

The boundary conditions and the initial conditions for this equation are

$$\theta = -C_w \qquad @\ Z = 0,$$
$$\theta = -C_w \qquad @\ \eta = 0. \quad (14)$$

Equation 13 may be rewritten in terms of dimensionless numbers as

$$\frac{\partial \theta}{\partial \eta} + \frac{\partial \theta}{\partial Z} = -2\left(\frac{Sh}{ReSc}\right)\frac{L}{r_0}\theta, \quad (15)$$

Equation 15 may be solved by the method of Laplace Transforms, resulting in

$$\theta = -C_w e^{-\beta Z} \qquad \text{for } Z < \eta$$
$$\theta = -C_w e^{-\beta \eta} \qquad \text{for } Z > \eta \quad (16)$$

where β is defined as

$$\beta = 2\left(\frac{Sh}{ReSc}\right)\frac{L}{r_0} \quad (17)$$

Substituting the result for long times into Eq. 11 ($\eta > 1$) and incorporating the initial condition $\phi = 1$ @ $\eta = 0$, the average dimensionless radius of the solid phase over the length of the film from 0 to L as a function of time is

$$\overline{\phi} = 1 + \frac{\overline{M}C_w}{2\rho_0}[1 - e^{-\beta}]\eta \qquad \text{for } Z < \eta \quad (18)$$

Substituting into the original equation for the mass of the film, the total mass of the film in terms of dimensionless time η is

$$M(\eta) = \rho_0 \pi L r_0^2 \left[\left(\frac{R}{r_0}\right)^2 - \overline{\phi}^2\right]. \quad (19)$$

The normalized film residual (mass of film remaining/mass of initial film) can be written as (Webb, 1994):

$$\frac{M(\eta)}{M(0)} = \frac{\left[\left(\frac{R}{r_0}\right)^2 - (1 + \kappa\eta)^2\right]}{\left[\left(\frac{R}{r_0}\right)^2 - 1\right]} \quad (20)$$

where

$$\kappa = \frac{\overline{M}C_w}{2\rho_0}[1 - e^{-\beta}]. \quad (21)$$

Incorporating the definitions for Re, Sc, and letting $Sh = a\,Re^b Sc^c$, an expression for the effect of bulk velocity on the rate of removal can be derived as:

$$\frac{\partial M(t)}{\partial t} = -\pi L r_o \overline{M}C_w \frac{[2^b a R^{b-1} v_z^b \rho^{b-1} Sc^{c-1}]}{\mu^{b-1}}. \quad (22)$$

The rate of removal of calcium phosphate thus depends on the velocity of the bulk fluid raised to the b power.

Experimental Procedure

A number of studies have been done on the removal of proteins (from milk fouling) from stainless steel surfaces. In contrast, the first phase of our research focuses on the removal of calcium phosphate residues representative of those formed during high-temperature processing (e.g., aseptic) of dairy based products. The experimental method consists of real-time solid scintillation measurements of the change in the beta emissions from radiolabeled residues coating the inner surface of a stainless steel tube. In an effort to model industrial pipe cleaning, the instantaneous rate of contaminant removal was studied in the region of fully developed turbulent flow. The heterogeneous P^{32} labeled calcium phosphate slurry used to coat the tube is a mixture of the compounds commonly found in milk fouling residues. Although prepared at temperatures lower than those found in high-temperature milk processing, the calcium phosphate slurries had Ca/P ratios representative of the formulations in fouling residues.

Experiments were performed on the decontamination of a heterogeneous calcium phosphate deposit over a range of experiment conditions (e.g., pH, flow rate). The results of these tests will be compared to the proposed dissolution model. The decontamination data is expected to deviate somewhat from the idealized dissolution model, especially since the calcium phosphate morphology is not well defined.

The following sections describe the experimental apparatus and the methods used to prepare calcium phosphate slurries. The chemical properties of the slurries (e.g., solubility, Ca/P ratio) and the physical nature of the resulting residues (e.g., morphology) were determined using a number of analytical techniques. The procedure developed for coating the stainless steel test cell is presented along with the verification of the coating uniformity. This is followed by a discussion of the decontamination experiments.

Apparatus

A system was designed to determine the rate of removal of calcium phosphate residues from the inside of stainless steel tubes. The apparatus consists of a tube cell coated with calcium phosphate through which solvent flows and a solid scintillation detector to measure beta emissions from P^{32} radiolabeled calcium phosphate films.

Flow System. The flow system in Figure 3a is composed of a fresh solvent storage tank, a waste solvent storage tank, a Micropump Model 101-415 pump, an Omega flow meter, a 304 stainless steel tube cell, and 304 stainless steel piping. The stainless steel tube cell fabricated by the Precision Engineering Shop at North Carolina State University was designed to allow a high transmission rate of beta particles. The cell consists of a thin inner tube (thickness = 0.1016 mm) and an outer protective tube (OD = 12.7 mm, length 60 mm) with a window opening for connection to the CaF_2 scintillator detector. The inner tube ID was equal to that of the connecting piping (10.5 mm). Tube cells were created with two types of surface finishes: a #4 finish, which is a finely polished surface, and a #63 finish, which is visibly rough.

Detection System. The solid-scintillation device (Figure 3b) measures the rate at which beta particles leave the tube cell. β-particles that are emitted from P^{32} have a maximum energy of 1.71 MeV. The percentage of transmitted β-particles is defined by:

$$N(t')/N(0) = \exp(-\mu_m t') \qquad (23)$$

where $N(0)$ is the number of incident beta particles, $N(t')$ is the number of beta particles transmitted through a thickness t', and μ_m is the mass absorption coefficient (Tsoulfanidis, 1983). Approximately 48% of the β-particles emitted from the film deposit on the window were able to pass through the stainless steel window.

The light signal from the CaF_2 scintillation detector (Bicron) is sent to a photo-multiplier tube (Bicron) where it is amplified and converted to an electronic signal. This signal is transmitted through a Tennelec TC145 preamplifier, a Tennelec TC241 amplifier, a multichannel scalar (Oxford) and a multichannel analyzer (Oxford). The multichannel scalar converts it to net counts. These two signals are sent in digital form to an IBM 386 compatible P/C, which displays and stores the signals for future analysis.

Calcium phosphate slurry preparation and decontamination procedure

Calcium phosphate films were created from a slurry of phosphoric acid and calcium hydroxide. One hundred μL of radiolabeled 2×10^{-7} M phosphoric acid (DuPont Chemical) and 100 μL of unlabeled 1 M phosphoric acid (Fisher Scientific) were mixed with 5.3 mL of a 1.057×10^{-2} M calcium hydroxide solution (Fisher Scientific). If the activity of the radiolabeled phosphoric acid was too high, the acid was diluted with reverse osmosis (RO) water until a safe level was reached. The mixture of phosphoric acid and calcium hydroxide was covered and allowed to equilibrate in a centrifuge tube for 24 h at approximately 25°C. The solution was centrifuged (Fisher Scientific; Marathon 6K) for 50 min at 5,000 rpm, the supernatant was drained, and the calcium phosphate slurry was dried under a 250-W infrared lamp (Fisher Scientific; Infra-Rediator) at approximately 89°C for 2 h. To create a well-mixed slurry, 2 mL of DI water was added to the centrifuge tube and the solution was stirred using a micro-stir bar for 15 min.

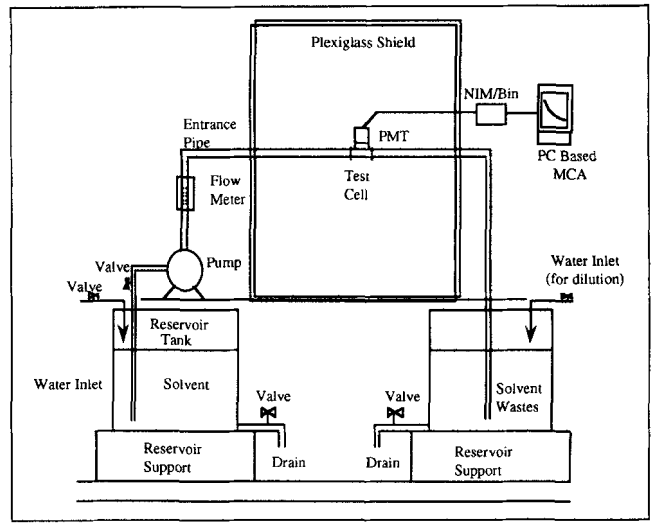

Figure 3a. Experimental flow system.

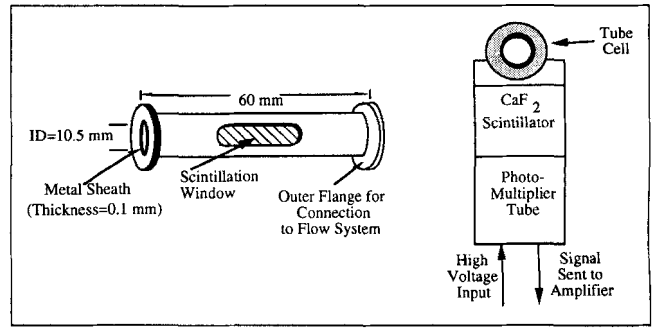

Figure 3b. Experimental tube cell.

To prepare the test cell for decontamination experiments, one mL of the reconstituted calcium phosphate slurry was injected into the stainless steel tube cell. Two techniques were used to dehydrate the slurry: rotational drying and stagnant drying. In rotational drying, the tube cell was rotated horizontally at 60 rpm under the 250 W infrared heat lamp at 89°C for 12 h. Stagnant drying was done by injecting one mL of the slurry into a tube cell mounted with the window face down. These samples were also dried at 89°C for 12 h.

To test the two coating techniques, a tube cell without a window was coated with radio labeled calcium phosphate and allowed to dry. These two cells were then compared by measured solid scintillation counts at various angles. A plot of these results can be seen in Figure 4. The half-life of P^{32} is 14 days; hence, the difference in net counts in these two experiments is a result of the differences in P^{32} activity. The stagnant coating has a standard deviation of 10.73%, whereas the rotational coating varies only 1.33% over the range of angles measured. The error associated with measuring the coatings is approximately 1.0%. By comparing the error of the rotational coating and the error of measurement, it was concluded that the rotational technique created an even coating in the theta direction within 0.34%.

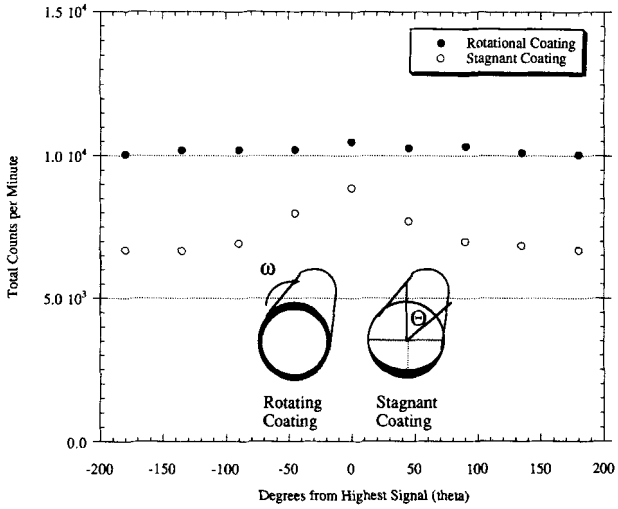

Figure 4. Distribution of calcium phosphate in experimental flow cell: rotational vs. stagnant coating techniques.

The flow cell used in this study did not have a window.

The average mass of calcium phosphate mixtures for coating the tube cell was 3.14 ±0.198 mg. The thickness of this mass t_{film} on the surface of the tube cell was estimated from the dimensions of the cell and the density of the material:

$$M = \rho\pi(R^2 - r_0^2)L \tag{24}$$

$$t_{film} = R - r_0 = 0.692\ \mu m \tag{25}$$

where M is the dry mass of the film deposited in the tube cell, ρ is the calcium phosphate density (2.306 g/cm^3), R is the radius of the tube cell, and r_0 is the initial distance from the center of the tube cell to the solid surface of the film. This value for r_0 was used for model calculations involving rotational coatings; it assumes that the calcium phosphate is evenly coated on the surface.

The tube cell was inserted into the flow apparatus so that the window was flush against the solid scintillation detector (Figure 3b). Once the tube cell was tightly secured, and before the flow was started, the activity of the coating was measured for one minute. The pump was turned on and activity measurements (net counts) were taken over 10 s intervals.

The length of the experimental run was limited by the size of the solvent reservoir (189 L) and the flow rate of the solvent (3.8–11.4 L/min). Water of various purity levels used to produce the cleaning solvent included: deionized water, reverse osmosis water, and tap water. A solution of 12.1 normal hydrochloric acid, HCl (Fisher Scientific) was added to the water to achieve the desired pH.

Solubility determination

Studies were performed using radio-labeled (P^{32}) calcium phosphate to determine equilibrium solution concentration (C_w) at room temperature. Samples were allowed to equilibrate for three weeks and then subjected to liquid scintillation measurements. Calcium phosphate was prepared in an identical manner to that used in coating the experimental flow cell. Calibration solutions were prepared by completely dissolving a given amount of calcium phosphate in a strongly acidic solution (pH = 2.0). Varying amounts of this calibration solution were then pipetted into a liquid scintillation cocktail (ICN; CytoScint) and counted using a liquid scintillator (Packard 1500 Tri-Carb Liquid Scintillation Analyzer).

Four solubility studies were performed with limited reproducibility. Figure 5 shows the results of these studies over the range of solution pH used in decontamination experiments. The experimental solubility is also compared with literature solubility values for brushite (Driesseus, 1990). It should be noted that our solubility experiments used the pH of the solvent before it was added to the calcium phosphate, whereas literature values found the pH of the solvent after equilibrium was reached. It can be seen that the solubility of brushite in the literature is higher than that of the calcium phosphate used in this study. This difference is most likely a result of the calcium phosphate being a mixture of brushite and hydroxyapatite and the fact that solvent pH values were calculated differently.

Ca/P ratio measurements for calcium phosphate precipitates

The literature states that calcium phosphates created under acidic conditions generally form brushite ($CaHPO_4 \cdot 2H_2O$ and hydroxyapatite $Ca_{10}(PO_4)_6(OH)_2$ (Driesseus and Verbeek, 1990). Brushite has a Ca/P ratio of 1.0 while the Ca/P ratio of hydroxyapatite is 1.67. Therefore, a solution with an initial $Ca(OH)_2/H_3PO_4$ ratio equal to 0.5 leads to a brushite-rich precipitate. Conversely, a solution with an initial $Ca(OH)_2/H_3PO_4$ ratio equal to 2.0 yields a hydroxyapatite-rich precipitate. The Ca/P ratio in milk deposits has been reported to be approximately 1.5 (Lyster, 1965; Jeurnink and Brinkman, 1994).

The calcium phosphate precipitates for the Ca/P ratio studies were obtained by reacting calcium hydroxide solution (lime water) and unlabeled o-phosphoric acid. The mixture was left undisturbed in a centrifugal tube for 24 h at room temperature. To measure Ca/P ratios, the precipitates were

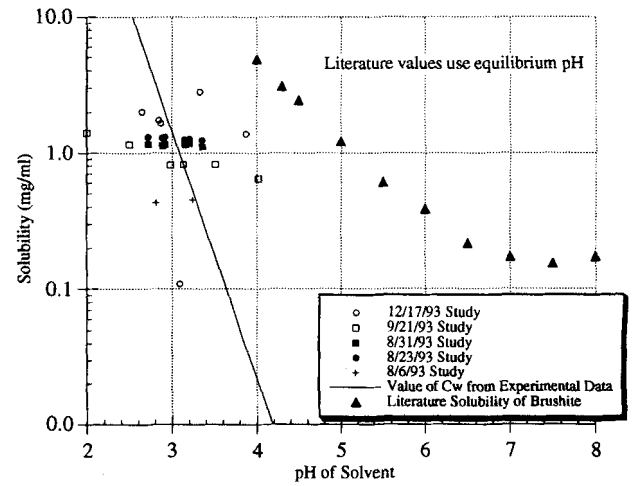

Figure 5. Changes in calcium phosphate solubility with pH.

Compared with literature solubility for brushite (Driesseus, 1990).

Table 1. Results of UV-Visible Spectrometry and Atomic Absorption Studies

$Ca(OH)_2$ (mmol)	H_3PO_4 (mmol)	$Ca(OH)_2/H_3PO_4$ Molar Ratio	Ca Precip. (mmol)	P Precip. (mmol)	Ca/P ratio of Precip.	Avg. Ca/P
0.1	0.2	0.5	0.0114	0.0114	1.000	
0.1	0.2	0.5	0.0112	0.0112	1.000	1.00
0.1	0.1	1.0	0.0711	0.0651	1.092	
0.1	0.1	1.0	0.0777	0.0678	1.146	1.12
0.1	0.05	2.0	0.0653	0.0441	1.481	
0.1	0.05	2.0	0.0763	0.0496	1.538	1.51

completely dissolved by adding 10 mL deionized water and 0.1 mL hydrochloric acid (12.1 Normal, Fisher Scientific Reagent Grade). The precipitates were analyzed for calcium and phosphorus contents using atomic absorption (AA) and UV-visible spectrometry, respectively; the results are shown in Table 1. When the molar ratios of $Ca(OH)_2/H_3PO_4$ were 0.5, 1.0, and 2.0, the Ca/P ratios of the resulting precipitates were determined to be 1.00, 1.12, and 1.51, respectively.

Analysis of supernatant solution

To ascertain which calcium phosphates were created, the solution in equilibrium with the precipitated calcium phosphate was analyzed. In this test calcium phosphate was made by mixing 100 μL of unlabeled 1 M phosphoric acid with 5.3 mL of 1.057×10^{-2} M calcium hydroxide solution. To compensate for the 100 μL of labeled phosphoric acid, 100 μL of DI water were added. This combination of calcium hydroxide and phosphoric acid yields an initial $Ca(OH)_2/H_3PO_4$ ratio of 0.56. The NCSU Soil Science Department performed inductively coupled plasma atomic emission (ICPAE) spectrometry analysis (Perk and Elmer; Plasma 2000) of various dilutions of supernatant in equilibrium with calcium phosphates with DI water. The supernatant was found to contain 222 ppm (7.17×10^{-3} M) phosphorus and was 305 ppm (7.62×10^{-3} M) calcium. The measured pH of the supernatant solution was 5.45.

Using a previous study on solubility isotherms developed for brushite (DCPD) at various solution pHs (Gregory et al., 1970), a phase diagram was created for calcium phosphates at 25°C. At the pH and calcium content in our supernatant, the precipitates appear to be in equilibrium with a supersaturated solution of brushite. Similar studies by Patel et al. (1974) found the calcium concentration of brushite in equilibrium with a solution having a pH of 5.41 to be 3.74×10^{-3} M, slightly lower than that in our study.

Results and Discussion

As discussed in the theoretical section, the mass-transfer model describes the molecular dissolution of calcium phosphate in a well defined flow field. Visual observation of the calcium phosphate films, however, indicates that the surface is not smooth or uniform in nature. Furthermore, the results reported here strongly suggest that the removal of the calcium phosphate is due to both residue dissolution and shearing of large chunks of the residues. In an effort to characterize the calcium phosphate surface morphology, scanning electron micrographs were taken of the surface of the residue. The SEM study will assist in any modification of the theoretical model to incorporate the effects of shear in cleaning.

Scanning electron microscopy (SEM) studies

Scanning electron microscopy studies were performed to investigate the morphology of the calcium phosphate films. Three different SEM studies examined (1) the effect of pH on dissolution, (2) the effect of drying temperature on film morphology, and (3) the effect of coating thickness on film morphology. SEM analysis could not be performed on a coated tube cell because the cells could not be opened for observation without disturbing or destroying the film. Stainless-steel coupons made of the same 304 stainless steel as the experimental tube cells (1 cm^2) were coated with calcium phosphate slurries and dried under an infrared heat lamp to evaporate the water producing a solid residue. Figure 6 shows the resulting calcium phosphate film without any treatment.

After drying, the coated stainless-steel samples were suspended in a well-mixed solution of distilled water and hydrochloric acid at 25°C. The constant bulk flow of the solvent was provided by a magnetic stirbar. After allowing the test coupons to remain in the bath for a set time, they were removed and allowed to dry overnight at room temperature. Scanning electron micrographs were taken of the dried samples.

The pHs of these solutions were selected based on the pH of solvents used in decontamination experiments. After 20 min of cleaning at a pH of 2.5, no particles of calcium phosphate are present and the stainless steel is visible (Figure 7a). Figure 7b represents five minutes of cleaning in a solution with a pH of 2.89; under these conditions, the majority of the

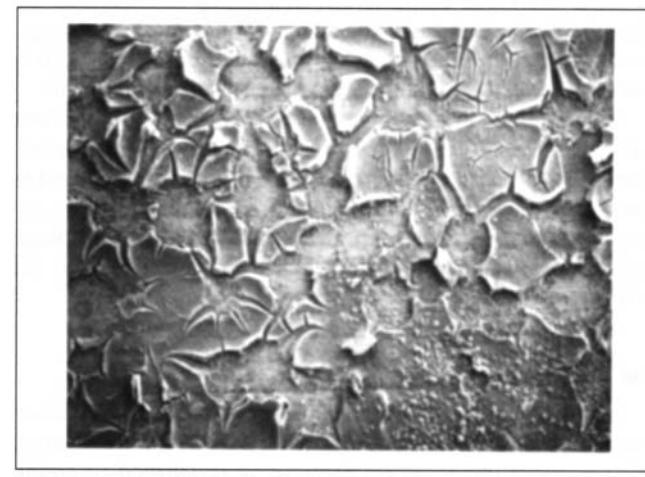

Figure 6. SEM calcium phosphate coating before cleaning.

30× magnification.

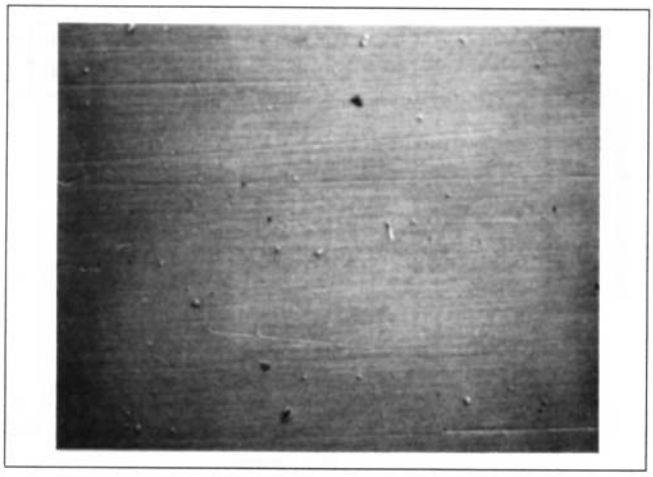

Figure 7a. SEM calcium phosphate coating after 20 min of cleaning at a pH of 2.5.
30× magnification.

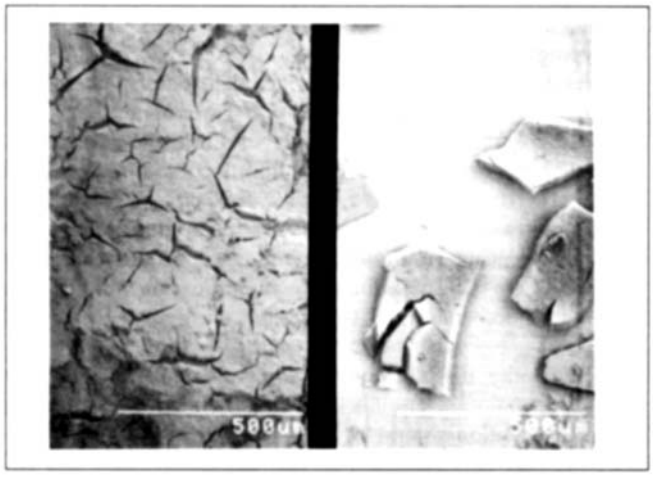

Figure 7b. SEM calcium phosphate coating after 5 min. of cleaning at a pH of 2.89.
30×/300× magnification.

calcium phosphate remained on the coupon surface. Approximately 50% of the calcium phosphate film has been removed after 20 min of cleaning under the same conditions. This reduction in cleaning can be attributed to the low solubility of calcium phosphate in high pH solvents.

To determine the effects of drying temperature on the morphology of the calcium phosphate coating, coupons were dried under an infrared heat lamp for 4 h at temperatures that matched those used in the preparation of the residues used in the decontamination studies (approximately 25, 80 and 150°C). Double coatings of calcium phosphate were prepared on stainless steel coupons. The first layer of slurry was dried under a heat lamp before the second slurry solution was added to the petri dish containing the stainless steel sample. Each layer of coating was dried at temperatures of 25, 80 or 150°C for 4 h under an infrared heat lamp. Figures 8 and 9 indicate that the macroscopic film morphology varied slightly over the temperature range studied. Figure 8 shows a double coating prepared at 25°C and Figure 9 is a double coating

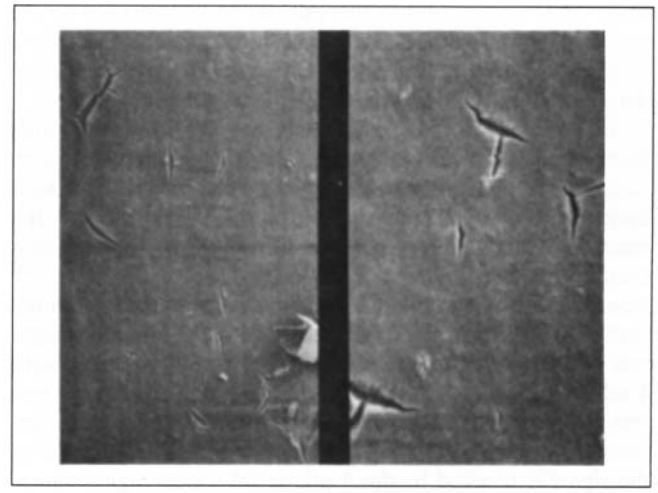

Figure 8. SEM double thickness coating of calcium phosphate coating dried at 25°C.
60×/300× magnification.

dried at 150°C. It should be noted that at the higher temperature the surface defects are not only more pronounced, but they are also larger and star shaped.

The calcium phosphate particle sizes were estimated from the SEM photographs taken in the cleaning studies. Eight crystals were selected to estimate the dimensions of an average crystal; the crystals were traced onto wax paper and the projected area was measured. From these estimates the projected surface area of crystals was found to range from 2.5×10^4 to 1.0×10^5 μm^2 with an average area of 6.5×10^4 μm^2.

Decontamination experiments

The effect of several parameters on the removal rate of calcium phosphate was studied including solvent type, flow rate, coating technique, solvent pH, drying temperature of tube cell, solvent temperature, coating thickness, and surface finish. The net counts detected by the solid scintillator were

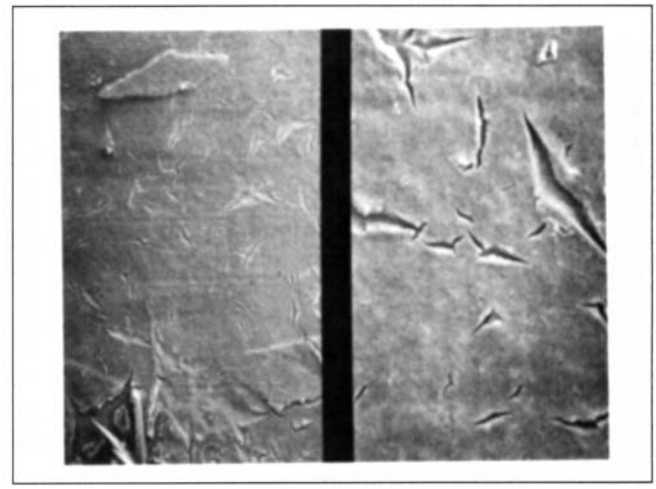

Figure 9. SEM double thickness coating of calcium phosphate dried at 150°C.
60×/300× magnification.

assumed to correspond to the calcium phosphate film on the window. When the tube cell is initially filled with water, there is an abrupt drop in the signal. This is because water is a low density material and absorbs the energy of beta particles.

An experiment was performed to measure the signal dampening associated with the solvent blocking beta particles. Performing a stationary test verified that this sudden drop was due to the dampening of the water and not the removal of large chunks of material from the surface initially. During this test, a flow cell was coated with 6.28 mg of P^{32} labeled calcium phosphate. The flow cell was then mounted vertically against a solid scintillator, and the signal strength was measured before and after the cell was slowly filled with 4 mL of DI water. There was essentially no shear in the system and the signal dropped significantly. For the coating prepared using the rotational technique, approximately 60% of the signal is blocked by the 4 mL of DI water. Signal dampening was not as pronounced (less than 10%) in stagnant coatings because the majority of the coating was on the side of the flow cell facing the detector; hence, most beta particles did not have to pass through solvent. This behavior was taken as an indication of role of the water in blocking the signal from the calcium phosphate on the far side of the flow cell.

Based on these dampening tests, the data collected during decontamination experiments were normalized to the signal strength after 30 s of solvent flow. 30 s was chosen to ensure that the flow and the corresponding dampening effect of the water were minimized. This normalized signal represents the fraction of the remaining P^{32}, which is proportional to the fraction of calcium phosphate remaining on the surface.

Experiments were conducted to gauge the reproducibility of experiments using RO water as the solvent. Four decontamination experiments were performed on stagnant coated tube cells using RO water flowing at 7.8 L/min (Figure 10). The pH of the solvent in these experiments ranged from 2.83 to 2.89. The largest deviation occurs at 400 s and is equal to approximately 10 percent deviation from the average. Figure 11 shows the decontamination of coatings prepared using the rotational technique; the solvent flow rate was 3.8 L/min and the average solvent pH was 2.88.

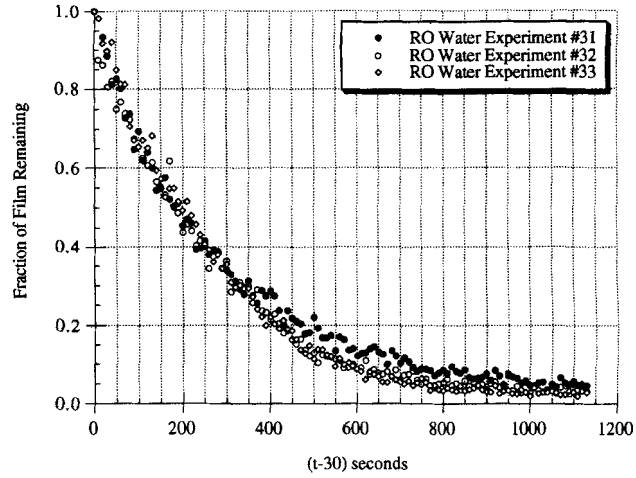

Figure 11. Reproducibility of RO water experiments with rotational coating, a solvent flow rate of 3.8 L/min, and an average solvent pH of 2.88.

Several experiments were conducted to determine the reproducibility of the decontamination experiments for both #63 and #4 finishes. Figure 12 suggests that the surface finish had little effect on both the initial decontamination rates and final decontamination rates for RO experiments. These studies indicated that the use of rotational coatings and RO water as a solvent resulted in consistent reproducible cleaning results. In all subsequent decontamination studies, the aforementioned conditions (rotational coating and RO water) were used.

Because the dissolution reaction is assumed to be fast enough to maintain equilibrium with the solute species, the rate of dissolution should be mass-transfer limited. In particular, the rate of dissolution should depend on how fast hydronium ions can reach the mass-transfer interface. This is confirmed by the experiments showing varying decontamina-

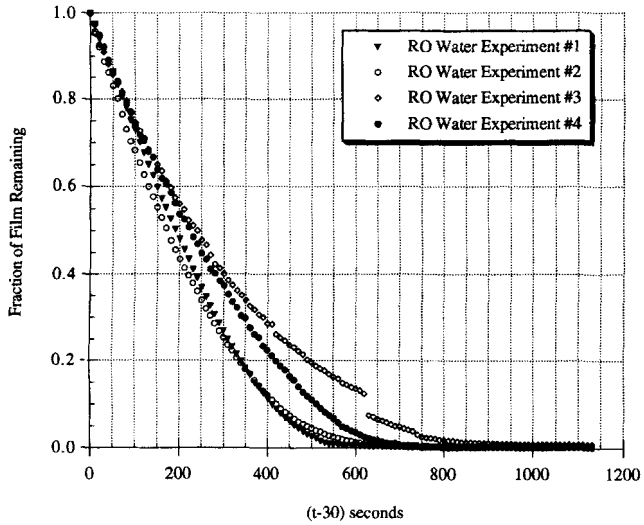

Figure 10. Reproducibility of RO water experiments with stagnant coating, a solvent flow rate of 7.6 L/min, and an average solvent pH of 2.85.

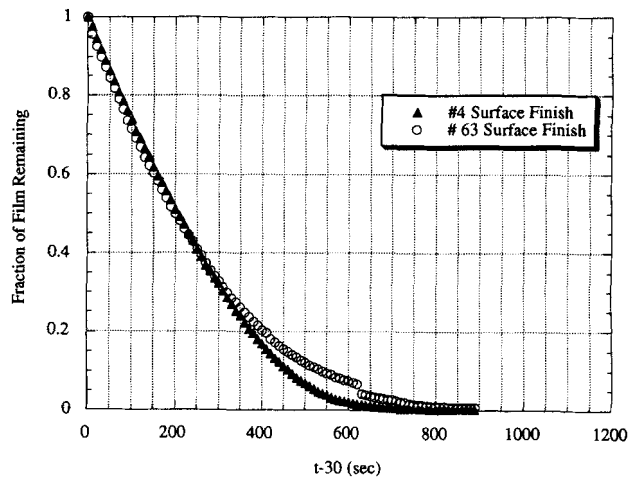

Figure 12. Effect of surface finish on RO water experiments with stagnant coating, a solvent flow rate of 7.6 L/min, and an average solvent pH of 2.86.

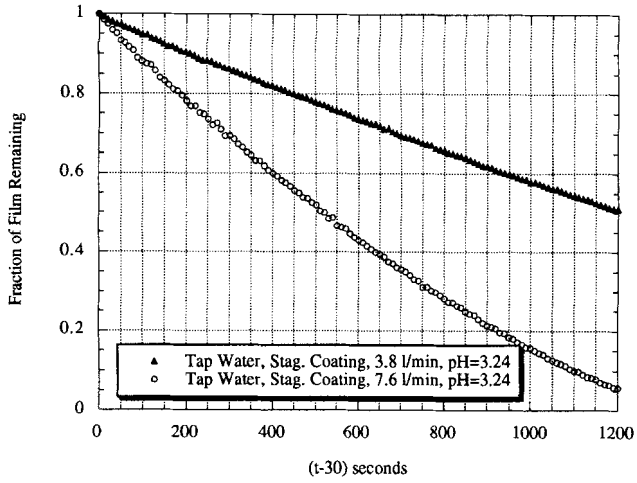

Figure 13. Effect of flow rate on tap water decontamination experiments with stagnant coating and an average solvent pH of 3.24.

tion rates with solvent flow rates. Initial decontamination rates were determined by performing a linear regression over the first 100 s of a particular decontamination experiment.

The effect of flow rate on decontamination rates for tap water experiments can be seen in Figure 13. The 3.8 L/min experiment had an initial decontamination rate of 0.052% removal/s, whereas the 7.6 L/min experiment was 0.127% removal/s; this corresponds to a 140% increase in cleaning rate. The effect of flow rate on decontamination rates for RO water experiments is illustrated in Figure 14. The values for initial decontamination rates can be seen in Tables 2 and 3. Increasing the RO water flow rate from 3.8 to 7.6 L/min and from 7.6 to 11.4 L/min corresponds to a 65% and a 25% increase, respectively, in the initial cleaning rate.

The solubility and hence the removal of calcium phosphate film is effected by the pH of the solvent. The increase in removal of calcium phosphate with decreasing pH can be attributed to the dependence of calcium phosphate solubility on pH. The effects of solvent pH on RO water experiments can be seen in Figure 15. Material removed in the first 100 s

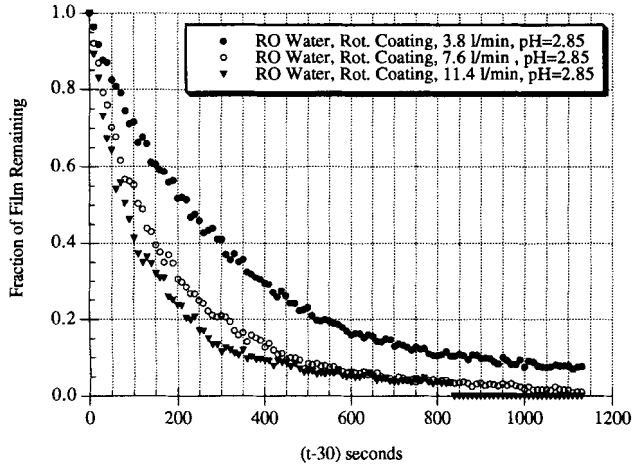

Figure 14. Effect of flow rate on RO water decontamination experiments with rotational coating and an average solvent pH of 2.85.

Table 2. Effect of Flow Rate on Initial Rate of Decontamination of RO and Tap Water Experiments

Flow Rate	Init. Decontam. Rate (% Removed/s) RO Water	Init. Decontam. Rate (% Removed/s) Tap Water
1	0.313	0.052
2	0.517	0.127
3	0.646	---

of cleaning was 25, 58, 59 and 66% for pH values of 3.24, 2.91, 2.86 and 2.82, respectively. The benefits of low pH on cleaning rates can also be seen at lower flow rates.

The effects of film thickness on decontamination rates for three RO water experiments conducted at 7.6 L/min at a pH of approximately 2.94 are presented in Figure 16. The various thicknesses were created by drying single layers one on top of another. Drying of each layer took place at 97°C for 4 h. It can be seen from this plot that the increase in film thickness decreases the initial rate of film removal. This contradicts the theory (Eq. 2) which predicts an increase in the initial rate of film removal with increasing film thickness due to decreasing film surface area with thicker coatings. A possible reason for the discrepancy is the fact that the multiple coatings were exposed to high temperatures for a different period of time prior to cleaning. The resulting tenacious film was more difficult to clean.

Comparison of dissolution model and experimental data

In the dissolution based mass-transfer model, a key parameter governing the theoretical removal rate is the calcium phosphate solubility. In spite of the variation in the experimental solubility data, an attempt was made to assess how well the model predicted changes in experimental conditions. Because of the scatter seen in experimental solubility studies, a value for C_w was derived from the dissolution model. This was performed by finding the average slope of the fractional remaining vs. time data from the decontamination experiments and calculating a value for C_w that provided a similar slope. A comparison between experimental data and the dissolution model has been made for both RO and tap water experiments. Figure 17 compares decontamination rates for RO experiments having a solvent pH of 2.85 and a flow rate of 7.6 L/min with the dissolution model (Eq. 20):

$$\frac{M(\eta)}{M(0)} = \frac{\left[\left(\frac{R}{r_0}\right)^2 - (1+\kappa\eta)^2\right]}{\left[\left(\frac{R}{r_0}\right)^2 - 1\right]}. \tag{20}$$

Table 3. Values of a Fit to RO Experiments

No. of Exp.	Solvent pH	Value of α
9	2.35	−0.00382
11	2.81	−0.00376
4	2.86	−0.00340
7	2.93	−0.00312
1	3.25	−0.00134
2	7.82	−0.000143

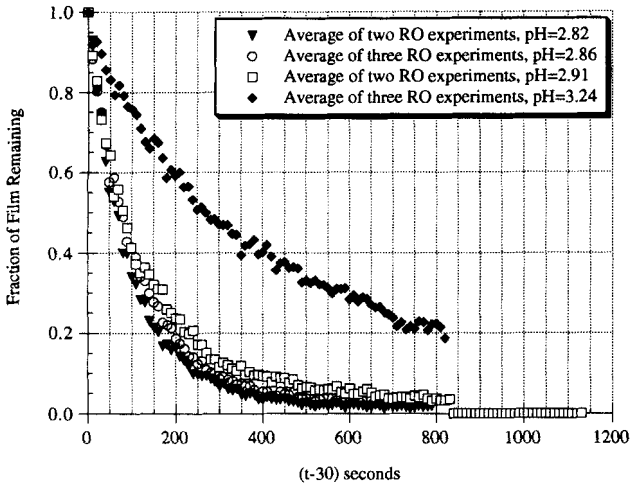

Figure 15. Effect of pH on RO water decontamination experiments with rotational coating, and a solvent flow rate of 11.4 L/min.

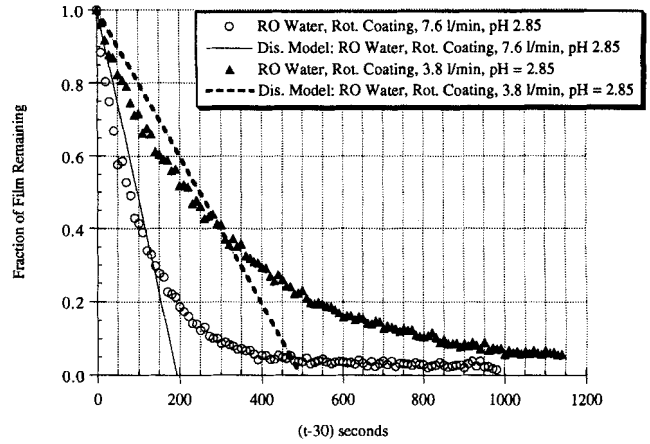

Figure 17. Dissolution model (Eq. 20) vs. RO water experiments with rotational coating, solvent flow rates of 3.8 and 7.6 L/min, and a solvent pH of 2.85.

It can be seen from this figure that there are differences in shape of the cleaning curve between the model and the experimental data. The experimental data is concave up, whereas the model tends to predict a rate of removal that increases slightly with time as the film surface area increases. Figure 17 also shows that the model slightly underpredicts initial cleaning rates and overpredicts cleaning rates over long periods of time. The difference between the model and the data early in the run may be because the actual surface area available for mass transfer may be larger than the predicted value ($2\pi rL$) due to an irregular morphology. The decrease in the rate of removal may be due to the reduced surface area due to the removal of calcium phosphate aggregates. It could also be caused by the adhesion of the residual or "baked on" calcium phosphate to the stainless steel. The model does show, however, the general trends in initial decontamination rates with changes in solvent flow rate and pH.

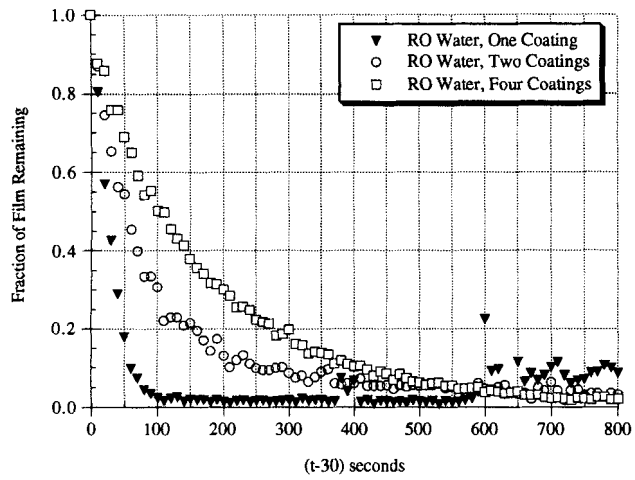

Figure 16. Effect of film thickness on RO water decontamination experiments with rotational coating, a solvent flow rate of 7.6 L/min, an average solvent pH of 2.94, and one, two and four coatings.

Comparisons between the model and tap water experiments performed at a solvent pH of 3.24 and a solvent flow rate of 3.8 and 7.6 L/min shows the model predicting removal rates higher than the actual experimental data. The reasons for these overpredictions is probably related to uncertainty in the coating thickness and variations in water quality.

Development of an empirical calcium phosphate decontamination model

The dissolution model assumes that the calcium phosphate residues are removed from the surface by molecular dissolution. This model does not account for the role of shear in removing large calcium phosphate aggregates. The SEMs suggest that during the cleaning process, large particles are dislodged from the substrate. Support for the supposition that both mechanical and dissolution mechanisms are involved in the removal of contaminant films has been observed in the literature. Jennings suggested that both mechanical cleaning and dissolution play a role in the cleaning of hard surfaces (Jennings, 1965; Linton and Sherwood, 1950; Harriott and Hamilton, 1965). Even though Jennings make it clear that both mechanical and dissolution mechanisms are important, most studies focus on a single mechanism.

Because of the difficulty in implementing the dissolution model, a numerical fit of our data has been made which incorporates the velocity and pH effects based on first-order models. The general form of the proposed rate equation is

$$\frac{dM}{dt} = -kM, \tag{26}$$

where k is a first-order rate constant. The form of Eq. 26 was chosen because: (1) the experimental data exhibited an exponential decay; and (2) the rate of cleaning of various fouled surfaces has been reported by several authors to have a first-order behavior (Jennings, 1957; Kern and Seaton, 1959; Gallow-LaVallee, 1982; Murray, 1987a,b). Equation 26 can be solved by using the following initial conditions:

$$M = M_0 \qquad @\ t = 0. \tag{27}$$

The following expression for the normalized mass results:

$$\frac{M(t)}{M_0} = \exp(-kt). \tag{28}$$

The first-order rate constant k can be expanded to account for the pH of the solvent, as well as the flow rate. Because the experimental data has been normalized to the mass of the film at 30 s (instead of the mass of film at $t = 0$), the least-square fit was performed using a function of the form:

$$\frac{M(t)}{M(30s)} = \exp[\alpha v_z^n (t - 30)], \tag{29}$$

where α and n were fitted parameters, v_z is the velocity of the fluid, and t is the time in seconds. The parameter α was fit separately for each unique solvent pH, so that a dependence of α on hydronium concentration could be determined. The parameters α and n were found by minimizing the sum of the squares of the relative error over the first 600 s of cleaning. All parameter fits were performed on RO experiments prepared using the rotational coating technique. The parameter n was found first by fitting both α and n to 27 experiments performed at pH values of 2.81, 2.86, and 2.93. A weighted average was found for n (0.70) and this value was used so that values of α could be found independently. Results of the fit for alpha can be seen in Table 3. After computing values for α, the parameter was then fit to Eq. 30; this form was selected based on the behavior of the data:

$$\alpha = a \exp(b[\mathrm{H}^+] + c) \tag{30}$$

where a, b, and c are constants. Equation 30 was fit by minimizing the sum of the square of the weighted-relative error. The weights were determined by the number of experiments representing each of the calculated α values; the results of this fit can be seen in Eq. 31:

$$\alpha = 0.008092 \exp(-371.272[\mathrm{H}^+] - 1.01692) \tag{31}$$

This procedure resulted in the following equation:

$$\frac{M(t)}{M(30s)} = \exp[\alpha v^{0.70}(t - 30)]. \tag{32}$$

Average errors were computed by averaging the errors found for each 10 s sample of fraction of film remaining in the set of experiments. The overall average error (6.7%) was found by weighting the average errors according to the number of experiments performed under the respective conditions.

Upon completion of the empirical equation, plots were constructed to compare the modified first-order model to the experimental data. Figure 18 compares the prediction of Eq. 32 to that of several average experimental runs at an average solvent pH of 2.86 and varying flow rates. Figure 19 compares the model empirical approximation with experimental runs at three solvent pH values and a flow rate of 11.4 L/min.

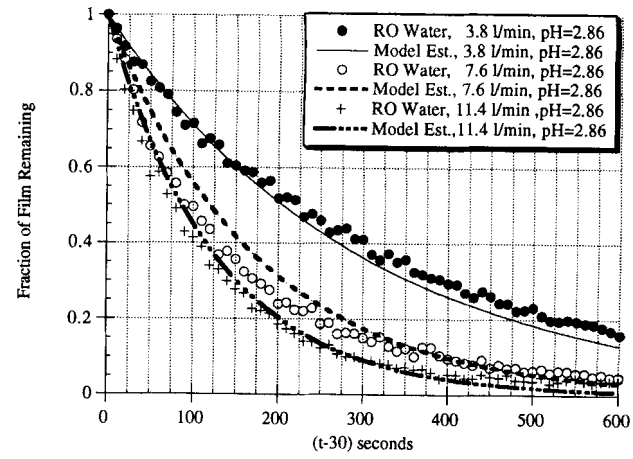

Figure 18. Empirical model (Eq. 32) vs. RO water experiments with rotational coating and a solvent pH of 2.86.

It can be seen from these plots that the first-order model predicts the removal of calcium phosphate relatively well; it does capture the trends found with changing solvent flow rate and pH. It should also be mentioned that some of the deviations in the fit may be traced back to scatter in the experimental data.

It was believed that a model of this type might elucidate the mechanisms involved in the removal of our calcium phosphate films by determining the effect velocity had on the cleaning rate. It is worth noting that the parameter n has a value less than 1.0. Kern and Seaton's model indicated that pure mechanical cleaning would result in the cleaning rate being proportional to the amount of kinetic energy the solvent possessed (Kern, 1959). They showed that cleaning from purely hydrodynamic effects (shear stress) would yield a cleaning rate with a velocity term to a power close to 2.0. A cleaning rate that is proportional to the velocity to the 0.70 power suggests that our system does has a strong dependence on dissolution based mechanisms.

In addition, the dissolution model developed suggests that if dissolution is the sole mechanism of removal, the removal

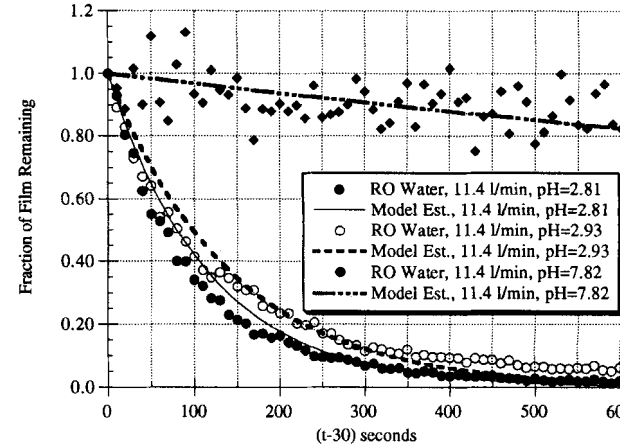

Figure 19. Empirical model (Eq. 32) vs. RO water experiments with rotational coating and a solvent flow rate of 11.4 L/min.

rate should be approximately proportional to the velocity to the 0.86 power. The dissolution model appears to predict the velocity trend more closely than that of a mechanical-based cleaning model, particularly in the initial portion of the cleaning process. However, the implementation of the model depends on the accuracy of solubility measurements.

Conclusions

The mass-transfer and hydrodynamic mechanisms governing the cleaning of contaminated surfaces are important in the development of efficient cleaning operations. This research has helped elucidate the mechanisms involved in the removal of calcium phosphate residues from the inside of stainless steel pipes. At the beginning of this project, it was assumed that calcium phosphate would be removed solely through the process of dissolution. The flow of solvent past the solid residues was though only to aid the removal of calcium phosphate by providing fresh solvent to the solid-liquid interface and a concentration gradient that would increase the dissolution rate. Several key research results in the current study have required a reevaluation of this hypothesis. First, SEM photographs of partially cleaned test coupons show that large aggregates of calcium phosphate have been detached from the surface of test coupons during the cleaning process. From these photographs, it was assumed that the calcium phosphate films were not removed solely by dissolution, but by a process that removed individual particles or chunks of calcium phosphate from the surface. It is believed that these particles are lifted from the hard surface by shear forces imparted by the fluid.

The second indication of the true nature of calcium phosphate removal came from the dissolution model that was developed from fundamental mass-transfer concepts. This model predicted that if dissolution was the only film removal mechanism, the rate of removal would actually increase slightly over time because of the increase in surface area in contact with the solvent as layers of contaminant were removed. The data from our decontamination experiments, however, showed that the rate of film removal did not increase over time, but instead showed a marked decrease. The dissolution based model, although theoretically sound, was difficult to test based on the lack of reliable solubility data. If, however, the solubility could be accurately determined, this model may overpredict the latter stages of calcium phosphate removal due to the adhesion of the heated residue to the stainless steel.

The dissolution model predicts the cleaning rate would be proportional to velocity raised to a power less than one. If mechanical cleaning were the only mechanism, the cleaning rate would be proportional to the kinetic energy of the fluid or the velocity to a power slightly less than two. Experiments have indicated that the cleaning rate is proportional to the velocity to the 0.70 power, suggesting that dissolution plays a significant role in the removal of calcium phosphate. The first-order model developed in this work provided an overview of the role of velocity and pH on the removal rate.

This research has provided insights into the mechanism of calcium phosphate removal by examining decontamination rates under various experimental conditions. It has also introduced a useful solid scintillation technique for obtaining a measurement of the mass of material remaining on a solid surface. Decontamination experiments have proven to be a reproducible means of estimating the film mass and its removal. The accuracy of the decontamination experiments is dependent upon the activity of the coating, the coating uniformity, and the initial mass of the coating. The technique used in decontamination experiments is adaptable; other materials may easily be substituted for calcium phosphate as long as radioactive labels are used that can penetrate the solid substrate (e.g., a thin barrier of stainless steel). The activity of the coating can be chosen based on the accuracy of the kinetic data that is desired.

Industries rarely see homogeneous contaminants, but instead a mixture of several compounds. It is recommended that a study of heterogeneous contaminants be conducted. It is unknown at this point whether or not the decontamination of the heterogeneous mixture could be predicted if a single component were radio-labeled and mixed with other unlabeled compounds. This type of prediction would be extremely beneficial because of the difficulty in labeling certain contaminants commonly found in industry. Specifically, predictions of this nature could be applied to studying the decontamination of actual deposits formed in milk processing.

Acknowledgments

Support by the Center for Aseptic Processing and Packaging Studies, an NSF-University-Industrial Center located at North Carolina State University, and the National Science Foundation, grant EID-9115327, is gratefully acknowledged. We also thank R. Carbonell for helpful technical advice, R. Caton and M. Britt for experimental assistance.

Notation

a, b, c = fitted dimensionless parameters (Eq. 30)
A = surface area of film, L^2
b_5 = rate constant, M/t (Eqs. 3, 4)
b_6 = rate constant, 1/t (Eqs. 3, 4)
C_b = bulk concentration of contaminant, moles/L^3
$C_{OH,B}$ = hydroxyl ion concentration in solvent, moles/L^3 (Eq. 1)
C_w = concentration of calcium phosphate at liquid-solid interface, moles/L^3
C_x = concentration of contaminant to be removed, mol/L^3 (Eq. 1)
D_{soil} = diffusivity of film, L^2/t (Eq. 2)
J = molar flux @ liquid-solid interface, moles/tL^2
k = arbitrary rate constant, t^{-1}, (Eqs. 7, 26), L^3/t mol (Eq. 1)
k_m = effective mass-transfer coefficient, L/t
k_1 = arbitrary rate constant, t (Eq. 5)
k_2 = arbitrary rate constant, L/t (Eq. 7)
L = length of mass-transfer region, L
M = mass of film, M
$M'(z)$ = local mass of film, M
M_0 = initial mass of film, M
$\overline{M}$ = average molecular weight of film, M/moles
n = fitted dimensionless parameter (Eq. 29)
N = moles of film, moles
$N(0)$ = number of incident beta particles (Eq. 23)
$N(t')$ = number of particles transmitted through thickness t' (Eq. 23)
r_0 = initial radius of liquid-solid interface, L
R = radius of pipe, L
Re = Reynolds number = $\rho vd/\mu$
R_i = radius of film, L
Sc = Schmidt number = $\mu/\rho D_{AB}$
Sh = Sherwood number = $k_m D/D_{AB}$
t = time, t
t' = thickness of window, L (Eq. 23)

t_{boun} = thickness of boundary layer, L (Eq. 2)
t_{film} = thickness of film, L
v = velocity of bulk solvent, L/t (Eq. 6)
$< v_z >$ = average fluid velocity, L/t^2
z = axial distance, L
z_w = thickness of oxide film, L (Eq. 7)
Z = dimensionless tube length, z/L (Eq. 12)

Greek letters

α = fitted parameter in Eq. 29
β = dimensionless variable, $\beta = 2(Sh/ReSc)L/r_0$ (Eq. 17)
η = dimensionless time, $\eta = t < v_z > /L$ (Eq. 12)
θ = concentration $(C_b - C_w)$, mol/L^3 (Eq. 12)
κ = dimensionless variable, $\kappa = (\overline{M}C_w/2r_0)(1 - e^{-\beta})$ (Eq. 21)
μ_m = mass absorption coefficient, L^2/M (Eq. 23)
μ = viscosity, M/Lt
ρ = density of solvent, M/L^3
ρ_o = density of film, M/L^3 (Eq. 9)
τ = shear stress, M/t^2L
$\underline{\phi}$ = dimensionless radius, R_i/r_o (Eq. 12)
$\bar{\phi}$ = average dimensionless radius, (Eq. 18)

Literature Cited

Bourne, M. C., and W. G. Jennings, "Some Physico-Chemical Relationships in Cleaning Hard Surfaces," *Food Tech.*, **15**, 495 (1962).

Corrieu, G., "State-of-the-Art of Cleaning Surfaces," *Fundamentals and Applications of Surface Phenomena Associated with Fouling and Cleaning in Food Processing*, B. Hallstrom, D. B. Lund, and C. Tragardh, eds., Tylosand, Sweden, Reprocentralen, Lund, Sweden, p. 90 (1981).

de Goederen, G., and N. J. Pritchard, "Improved Cleaning Processes for the Food Industry," *Fouling and Cleaning in Food Processing*, H. G. Kessler and D. B. Lund, eds., Druckerei Walch, Augsburg, Germany, p. 115 (1989).

Driesseus, F. C. M., and R. M. H. Verbeek, "The Calcium Rich Compounds of the System $Ca(OH)_2$-H_3PO_4-H_2O," *Biominerals*, CRC Press, New York, p. 37 (1990).

Gallot-LaVallee, T., M. LaLande, and G. Corrieu, "An Optical Method to Study the Kinetics of Cleaning Milk Deposits by Sodium Hydroxide," *J. Food Eng.*, **5**, 131 (1982).

Gotham, S. M., P. J. Fryer, and A. Pritchard, "Model Studies of Food Fouling," *Fouling and Cleaning in Food Processing*, H. G. Kessler and D. B. Lund, eds., Druckerei Walch, Augsburg, Germany, p. 1 (1989).

Grasshoff, A., "Environmental Aspects of the Use of Alkaline Cleaning Solutions," *Fouling and Cleaning in Food Processing*, H. G. Kessler and D. B. Lund, eds., Druckerei Walch, Augsburg, Germany, p. 107 (1989).

Gregory, G. M., E. C. Moreno, and W. E. Brown, "Solubility of $CaHPO_4 \cdot 2H_2O$ in the System of $Ca(OH)_2$-H_3PO_4-H_2O at 5, 15, 25 and 37.5°C," *J. Res. Nat. Bur. of Std.*, **74A**(4), 461 (1970).

Harper, W. J., *Sanitation in Dairy Food Plants*, Avi Publishing, Westport, CT (1972).

Harriott, P., and R. M. Hamilton, "Solid-Liquid Mass Transfer in Turbulent Pipe Flow," *Chem. Eng. Sci.*, **20**, 1073 (1965).

Jackson, A. T., "Cleaning Characteristics of a Plate Heat Exchanger Fouled with Tomato Paste using 2% Caustic Soda Solution," *U.K. Nat. Conf. on Heat Transfer*, Univ. of Leeds, Pergamon Press, p. 465 (1984).

Jennings, W. G., A. A. McKillop, and J. R. Luick, "Circulation Cleaning," *J. Dairy Sci.*, **40**, 1471 (1957).

Jennings, W. G., "Theory and Practice of Hard Surface Cleaning," *Adv. Food Res.*, **14**, 325 (1965).

Jeurnink, T. J. M., and D. W. Brinkman, "The Cleaning of Heat Exchangers and Evaporators After Processing Milk or Whey," *Int. Dairy J.*, **4**, 347 (1994).

Kern, D. Q., and R. E. Seaton, "A Theoretical Analysis of Thermal Surface Fouling," *British Chem. Eng.*, **12**, 258 (1959).

Lalande, M., and F. Rene, "Fouling by Milk and Dairy Product and Cleaning of Heat Exchange Surfaces," *Fouling Science and Technology*, L. F. Melo et al., eds., Kluwer Academic Publishers, Norwell, MA, p. 557 (1988).

LeClercq-Perlat, M. N., and M. LaLande, "A Review on the Modeling of the Removal of Porous Contaminants Deposited on Heat Transfer Surfaces," *Int. Chem. Eng.*, **31**(1), 74 (1991).

Lenges, J., "Study of Diffusion Coefficients for a Surfactant and of the Kinetics of Micellization of a Colorant," ScD Thesis, Univ. of Brussels (1982).

Linton, W. H., and T. K. Sherwood, "Mass Transfer from Solid Shapes to Water in Streamline and Turbulent Flow," *Chem. Eng. Prog.*, **46**, 258 (1950).

Lund, D., and C. Sandu, "State-of-the-Art of Fouling: Heat Transfer Surfaces," *Fundamentals and Applications of Surface Phenomena Associated with Fouling and Cleaning in Food Processing*, B. Hallstrom, D. B. Lund, and C. Tragardh, eds., Tylosand, Sweden, Reprocentralen, Lund, Sweden, p. 27 (1981).

Lyster, R. L. J., "Effects of Heating on Food-Stuffs," *Milk and Dairy Products*, Elsevier Applied Science Publishers, London, p. 353 (1979).

Lyster, R. L. J., "The Composition of Milk Deposits in an Ultra-High-Temperature Plant," *J. Dairy Res.*, **32**, 203 (1965).

Murray, A. P., "Mathematical Modeling of the Chemical Decontamination of Boiling Water Reactor Components," *Nucl. Technol.*, **79**, 359 (1987a).

Murray, A. P., "Modeling Nuclear Decontamination Processes," *Nucl. Technol.*, **77**, 194 (1987b).

Patel, P. R., T. M. Gregory, and W. E. Brown, "Solubility of $CaHPO_4 \cdot 2H_2O$ in the Quaternary System of $Ca(OH)_2$-H_3PO_4-NaCl-H_2O at 25°C," *J. Res. Nat. Bur. of Std.*, **78A**(6), 675 (1974).

Perka, A. T., C. S. Grant, and M. R. Overcash, "Waste Minimization in Batch Vessel Cleaning," *Chem. Eng. Commun.*, **119**, 167 (1993).

Plett, E. A., "Relevant Mass Transfer Mechanisms during Rinsing," *Fouling and Cleaning in Food Processing*, D. B. Lund, E. A. Plett and C. Sandu, eds., Univ. of Wisconsin, Madison, p. 395 (1985).

Sandu, C., "Chemical Reaction Fouling due Milk: Defects-Growth Model," *Fouling and Cleaning in Food Processing*, H. G. Kessler and D. B. Lund, eds., Druckerei Walch, Augsburg, Germany, p. 46 (1989).

Sandu, C., and D. Lund, "Fouling of Heating Surfaces—Chemical Reaction Fouling Due to Milk," *Fouling and Cleaning in Food Processing*, D. B. Lund, E. A. Plett and C. Sandu, eds., Univ. of Wisconsin, Madison, p. 122 (1985).

Sandu, C., and R. K. Singh, "Energy Increase in Operation and Cleaning Due to Heat-Exchanger Fouling in Milk Pasteurization," *Food Technol.*, **45**(12), 84 (1991).

Schlussler, H. J., "Cleaning of Hard Surfaces in the Food Industry," *Milchwissenschaft*, **25**(3), 133 (1970).

Timperley, D. A., and C. N. M. Smeulders, "Cleaning of Dairy HTST Plate Heat Exchangers: Comparison of Single- and Two-Stage Procedures," *J. of Soc. of Dairy Tech.*, **40**(1), 4 (1987).

Timperley, D. A., "The Effects of Reynolds Number and Mean Velocity of Flow on the Cleaning in-Place of Pipelines," *Fundamentals and Applications of Surface Phenomena Associated with Fouling and Cleaning in Food Processing*, B. Hallstrom, D. B. Lund, and C. Tragardh, eds., Tylosand, Sweden, Reprocentralen, Lund, Sweden, p. 402 (1981).

Tsoulfanidis, N., *Measurement and Detection of Radiation*, New York, Hemisphere (1983).

Webb, G., "Kinetics and Modeling of Calcium Phosphate Film Decontamination from Hard Surfaces," MS Thesis, North Carolina State Univ., Raleigh (1994).

Wennerberg, J., "Observations on the Behaviour of Fouling and Cleaning in Industrial Processes," *Fundamentals and Applications of Surface Phenomena Associated with Fouling and Cleaning in Food Processing*, B. Hallstrom, D. B. Lund, and C. Tragardh, eds., Tylosand, Sweden, Reprocentralen, Lund, Sweden, p. 76 (1981).

Manuscript received Nov. 23, 1994, and revision received Apr. 3, 1995.